7th International Conference on the Durability of Concrete Structures
20-22 May **2022**
University of Jinan, Jinan, Shandong, China

Numerical investigation on aggregate settlement and its effect onthe durability of hardened concrete

Yuxin Cai, Qing-feng Liu*
School of Naval Architecture, Ocean and Civil Engineering, Shanghai Jiao Tong University
Shanghai Key Laboratory for Digital Maintenance of Buildings and Infrastructure, Shanghai Jiao Tong University
* Corresponding author.
E-mail address: liuqf@sjtu.edu.cn (Q.-f. Liu).

ABSTRACT

Vibrating consolidation process is widely applied to field construction of cement concrete. However, high- frequency vibration can easily lead to the settlement of coarse aggregates (CAs) and then affects the durability of hardened concrete. This study has developed a 3-D concrete model to investigate the CA settlement caused by vibration and its effect on long-term chloride transport in concrete. Based on the proposed model, the influence mechanism of CA settlement on both chloride concentration distribution and initiation time of reinforcement corrosion is discussed in detail. The results indicate that due to the settlement, a more obvious fluctuation of chloride concentration along the height direction of concrete specimen can be observed with the increase of vibration time. According to the model prediction, the corrosion of the top steel bar initiates 1.03–1.80 years earlier than that of the bottom steel bar under different vibration time. The proposed model provides a new method to probe into the influence of vibration-induced settlement on chloride ingress in hardened concrete.

1. INTRODUCTION

The stability of fresh concrete refers to its ability to maintain the uniform distribution of constituents during transport, casting and compacting (Roussel, 2006). In the process of consolidation, vibration helps to remove entrapped air voids and improve the compactness of concrete, but also causes the relative movement and redistribution of various components of mixtures due to the insufficient cohesion and density difference (Ashraf et al., 2022). Notably, high-frequency vibration-induced settlement of coarse aggregates (CAs) greatly increases the heterogeneity of fresh concrete, which is usually reflected in the variation of CA volume fraction along the height direction.

The CA settlement caused by vibration has an adverse effect on the mechanical strength and especially long-term durability of hardened concrete. Gao et al. (2019) reported that both mechanical performance and chloride permeability variations along the casting direction tended to increase linearly with the degree of CA settlement, and the maximum difference rates of the two could reach 12.4% and 72.1%, respectively. Panesar and Shindman (2012) pointed out that concrete cast with quality materials and mix proportions in accordance with current guidelines might still be vulnerable to poor segregation resistance, which might result in negative impact on the transport properties and durability performance. In authors' prior work (Cai et al., 2020), it was found that due to the occurrence of CA settlement, when the height of concrete sample increased from 150 mm to 750 mm, the chloride migration coefficient increased by 50%, which was one of the reasons for the earlier corrosion initiation of reinforcement at a higher position.

Due to the opacity of concrete, the visual observation of CA settlement with naked eye is impossible. Therefore, some special experimental methods and techniques have been proposed to indirectly characterize the settlement phenomenon, such as image processing (Navarrete and Lopez, 2017), electrical conductivity (Khayat et al., 2003), ultrasonic velocity (Benaicha et al., 2015) and gamma-ray attenuation (Gokce et al., 2018). In recent years, the numerical models have been extensively used in the field of civil engineering with the rapid development of computer science and numerical algorithms. However, these developments have not been applied on the evaluation of CA settlement, and most knowledge is still based on experimental observations. Moreover, the experimental investigations on the durability of reinforced concrete in chloride-containing environments are time-consuming and expensive, which is also a concern that needs to be considered.

This study aims to develop a rational and reliable numerical model to investigate the vibration-induced CA settlement and its effect on the long-term durability of concrete. Based on the proposed model, the influence mechanism of CA settlement on both chloride profile distribution along the height direction and initiation time of reinforcement corrosion is further discussed. The numerical model proposed in this study provides a potential approach to visualize the CA movement and a theoretical method to probe into the influence of CA settlement on chloride ingress in hardened concrete.

2. THEORETICAL METHODS

2.1. CA settlement

It is generally believed that the yield stress can prevent CAs from settling in an undisturbed mortar matrix (Petrou et al., 2000), but the yield stress is known to decrease to a very low value or even disappear at vibrating state and the plastic viscosity plays a decisive role in the settlement of CAs at this time (Banfill et al., 1999). Assuming that the yield stress is reduced to zero, a single CA particle is mainly subjected to three forces: gravity, buoyancy and viscous resistance in vibrated mortars. The force analysis of the CA is presented in Figure 1.

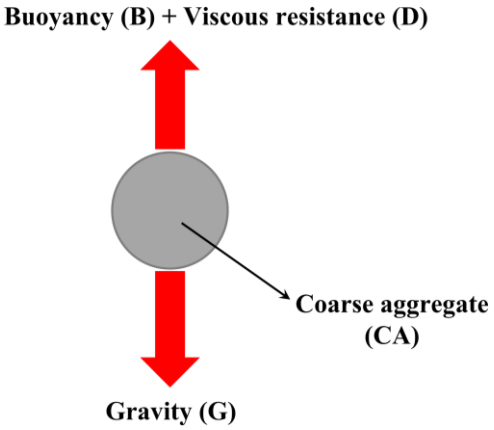

Figure 1. Force analysis of the CA in vibrated mortars.

Gravity (G), buoyancy (B) and viscous resistance (D) can be expressed by Equations (1)–(3), respectively.

$$G = \frac{1}{6}\pi\rho_a d^3 g \quad (1)$$

$$B = \frac{1}{6}\pi\rho_m d^3 g \quad (2)$$

$$D = 3\pi\eta v d \quad (3)$$

where ρ_a and ρ_m are the densities of CAs and mortars, and they are measured as 2.67 g/cm^3 and 2.28 g/cm^3 in the experiment. d is the CA particle size (5–20 mm), g is the gravitational acceleration (9.8 m/s^2), η_{pl} is the plastic viscosity of mortars, and v is the CA velocity.

Through integral calculation, the relationship between the vertical settlement height and vibration time can be derived as:

$$\Delta h = \frac{d^2 g(\rho_a - \rho_m)}{18\eta_{pl}} \cdot \left\{ t - \frac{d^2\rho_a}{18\eta_{pl}} \cdot \left[1 - \exp\left(-\frac{18\eta_{pl}}{d^2\rho_a} \cdot t \right) \right] \right\} \quad (4)$$

where Δh is the settlement height of the CA, and t is the vibration time.

Since the particle size of CAs is usually on the scale of 10^{-3} m, the constant and exponential terms in Equation (4) are much smaller than the linear term. Hence, the CA settlement height can be further expressed as:

$$\Delta h = \frac{d^2 g(\rho_a - \rho_m)}{18\eta_{pl}} \cdot t \quad (5)$$

Equation (5) shows the settlement height of a single CA in vibrated mortars. But, in fact, each CA particle is also subjected to the interaction from other ones. In this case, the plastic viscosity of mortars can be approximately replaced by that of concrete mixtures, so as to consider the interaction between the CA particles. Furthermore, the plastic viscosity of fresh concrete needs to be calibrated, because the Bingham model is no longer completely suitable to characterize the rheological behaviour of fresh concrete under the action of vibration. Consequently, the settlement height of the CA can be revised to:

$$\Delta h' = \frac{d^2 g(\rho_a - \rho_m)}{18k\eta_{pl}'} \cdot t \quad (6)$$

where, $\Delta h'$ is the actual settlement height of the CA, η_{pl}' is the plastic viscosity of fresh concrete (45.0 Pa·s), and k is the non-dimensional calibration coefficient for η_{pl}'. The specific value of k will be determined in Section 3.2.

2.2. Chloride transport

Diffusion describes the transport process of chloride ions from a high concentration area to a low concentration area in saturated concrete, which can be articulated by Fick's second law, as show in Equation (7).

$$\frac{\partial C}{\partial t} = D_{Cl}\frac{\partial^2 C}{\partial x^2} \quad (7)$$

where C is the chloride concentration, t is the diffusion time, D_{Cl} is the diffusion coefficient of chloride ions, and x is the diffusion depth.

Some empirical or theoretical equations have been developed to calculate the chloride diffusivity in cement mortars. This work adopts the generalized effective medium theory and develops the diffusion coefficient of cement mortars D_{cm} as follows (Zheng and Zhou, 2008; Du et al., 2015):

$$D_{cm} = \frac{2\varphi^{2.75} D_0}{\varphi^{1.75}(3-\varphi) + 14.44(1-\varphi)^{2.75}} \quad (8)$$

where φ is the porosity of cement mortars (38.64%), and D_0 is the ionic diffusivity in pore solution.

Note that a part of the chlorides diffusing through concrete can be bound in the hydration products. Here, Langmuir isotherm is used in the modelling to characterize the chloride binding effect.

$$C_b = \frac{\alpha \cdot C_f}{1 + \beta \cdot C_f} \quad (9)$$

where C_b and C_f are the bound and free chloride concentrations, and α = 0.42 and β = 0.8 L/mol are the binding coefficients determined by the experiment (Sergi et al., 1992).

Apart from the chloride ions focused in this study, there are some other ionic species existing in pore solution, including sodium, potassium, hydroxide, calcium, sulphate, etc. (Liu et al., 2015). Due to the differences in the charge properties and diffusion rates of various ions, it will generate charge imbalance between multi-species in local area of the concrete, which may affect the transportation of every ionic species (Chen et al. 2021; Meng et al. 2021; Meng et al. 2022; Liu et al. 2022). Mathematically, Nernst–Planck equation expresses the flux of ions in a multi-species pore solution, as follows:

$$J_k = -D_k \nabla C_k - \frac{z_k F}{RT} D_k C_k \nabla \Phi \quad (10)$$

Here, J_k, D_k, C_k and z_k represent the ionic flux, diffusion coefficient, ionic concentration and charge number of the k-th ion, respectively, F is the Faraday constant (96485 C/mol), R is the ideal gas constant (8.314 J/(mol·K)), T is the absolute temperature (298 K), and Φ is the electrostatic potential determined by Poisson's equation (see Equation (11)).

$$\nabla^2 \Phi = -\frac{F}{\varepsilon_0 \varepsilon_r} \sum_{k=1}^{N} z_k C_k \quad (11)$$

where ε_0 is the permittivity of vacuum (8.85×10^{-12} F/m), and ε_r is the relative permittivity of water at the temperature of 298 K (78.3).

3. MODELLING

3.1. Model foundation

In this study, a 3-D concrete model is established at mesoscopic level, as illustrated in Figure 2. The prismatic concrete specimen is in the size of 150 mm × 150 mm × 500 mm. The particle size of spherical CAs in the geometric model is 5–20 mm, which is randomly generated according to the Fuller curve, and the volume fraction of CAs is 45%. These parameters are the same as the experiments.

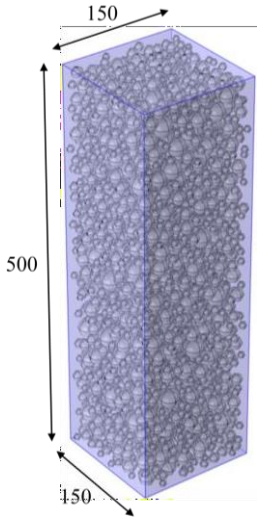

Figure 2. Schematic diagram of the 3-D concrete model (unit: mm).

The concrete specimen is simulated to be immersed in a marine environment with a sodium chloride concentration of 5 wt%. One side surface of the specimen is treated as an exposed surface, and other surfaces are set to be non-flux to ensure the one-dimensional transport of chloride ions in concrete. In addition, it should be noted that concrete pore solution is an environment with many types of ionic species. In this study, only sodium, potassium, chloride and hydroxide ions are analysed to characterize the electrochemical coupling effect between them, since the concentrations of other ionic species are rather low in the pore solution of concrete (Yu et al., 2021; Li et al., 2021; Li et al., 2022; Hu et al., 2023). Table 1 provides the various parameters of these ionic species used in the current model.

Table 1. Various parameters of the ionic species used in the current model.

Ionic species	Charge number	Diffusion coefficient in the pore solution	Initial concentration
Sodium	1	0.66×10^{-10} m²/s	190 mol/m³
Potassium	1	0.98×10^{-10} m²/s	380 mol/m³
Chloride	–1	1.07×10^{-10} m²/s	0 mol/m³
Hydroxide	–1	1.63×10^{-10} m²/s	570 mol/m³

3.2. Model calibration

Theoretically, the final height position of the CA after settlement can be expressed by Equation (12) through the previous calculation and derivation.

$$h' = h - \frac{d^2 g(\rho_a - \rho_m)}{18 k \eta_{pl}'} \cdot t \quad (12)$$

where h is the initial height position of the CA, and h' is the final height position of the CA after settlement.

Note that the CAs with different particle sizes have a different settlement rate, which will cause some of them to intersect in the model. To this end, the whole vibration process is divided into many short-time parts, and the vibration time of each step is set as 0.05 s. The final settlement model is generated by superposition of each part step by step, until the expected vibration time is reached. At the end of each part, if the CAs intersect, the involved ones are randomly bounced to the nearby empty space and the minimum distance between the CA surfaces is set as 100 μm.

In the model, the parameter information of every CA particle can be easily determined at any time and any position. The 3-D model is equally divided into five layers along the height direction, and all CAs are distributed in each layer based on the final position of the centre height of them. According to Equation (13), the CA volume percentage of each layer in the model can be calculated.

$$p_i = \frac{V_i}{V}(i = 1, 2, 3, 4, 5) \quad (13)$$

where P_i is the volume percentage of CAs in the i-th layer, V_i is the volume of CAs in the i-th layer, and V is the total volume of all CAs in the model.

At the same time, a method of segmented sieving was put forward to evaluate the settlement of CAs in the experiment (Cai et al. 2021). Here, a prismatic wooden mould with a cross section of 150 mm × 150 mm and a height of 500 mm was customized. In the test, the right amount of fresh concrete was poured into the mould. The specimens were vibrated for 5 s, 15 s and 25 s, respectively. After the vibration, the top of the mould was covered with a wooden board and fastened with bolts. Then the mould was slowly rotated by 90° from the original position, and the side wall was taken off. Next, four pieces of metal slides were inserted vertically along the designed iron grooves. The concrete mixtures were equally divided in five layers along the casting direction. Subsequently, the cover and partitions were removed in proper order. Concrete mixtures of each layer were poured into a 4.75 mm sieve to rinse to remove mortars. Finally, the residual CAs were dried and weighed to calculate the CA mass percentage of each layer in the specimen (see Equation (14)).

$$P_i' = \frac{m_i}{M}(i = 1, 2, 3, 4, 5) \quad (14)$$

where P_i' is the mass percentage of CAs in the i-th layer, m_i is the mass of CAs in the i-th layer, and M is the total mass of all CAs in the specimen.

Since the density of all CAs is the same, the volume percentage of CAs in each layer (P_i) can be fitted with the mass percentage (P_i') according to the segmented sieving results to calculate the calibration coefficient (k) used in Equation (6). The algorithm flow chart of k and correlation coefficient (R^2) is presented in Figure 3. It can be predicted that the value of R^2 will increase firstly and then decrease with the increase of k, that is, there is a peak value of R^2. When R^2 reaches its maximum value, the algorithm ends. It is found that when k is 0.62, the results of numerical model and experiment are in the best agreement. In that case, R^2 is 0.9865.

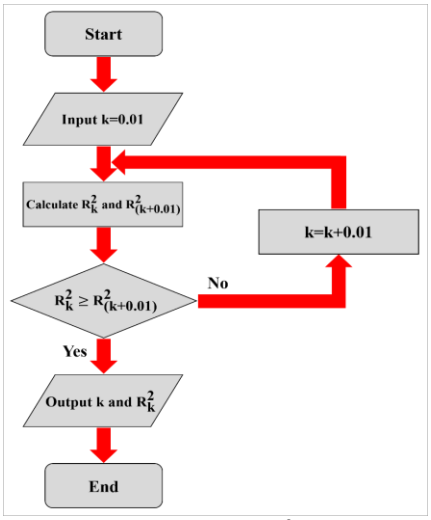

Figure 3. Algorithm flow chart of k and R^2.

4. RESULTS AND DISCUSSION

4.1. Visual analysis of CA settlement

Figure 4 depicts the variation of CA distribution with vibration time in the 3-D settlement model. It could be seen that with the progress of vibration, CAs gradually deposited to the bottom part of specimen, and the distribution profiles presented an increased content of CAs towards the bottom layer. For a single CA, the CA with a larger particle size showed a more notable settlement distance. It was noteworthy that the CA content in the top part of specimen was significantly decreased, especially when the vibration time reached 25 s, there were most of mortars and only few of small-sized CAs in the top 50 mm-height area (see Figure 4(c)).

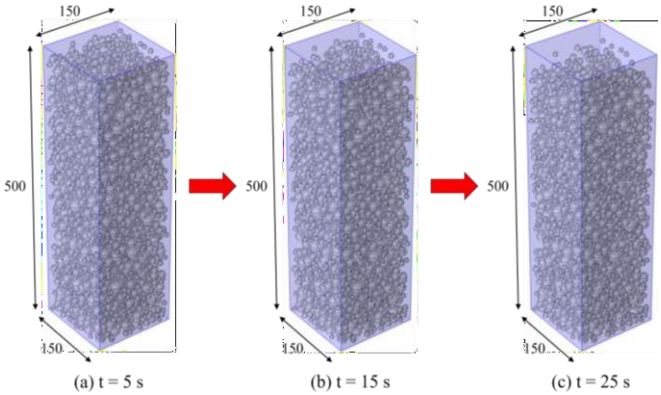

Figure 4. Visual analysis of CA settlement induced by vibration.

On the basis of the 3-D settlement model, the volume percentages of CAs in the five layers were calculated, as illustrated in Figure 5. Evidently, as the vibration time increased, the heterogeneity of CA distribution along casting direction was gradually strengthened, which was reflected in the obvious decrease of CA content in the top part and the increase of that in the bottom part. This was consistent with the direct observation shown in Figure 4.

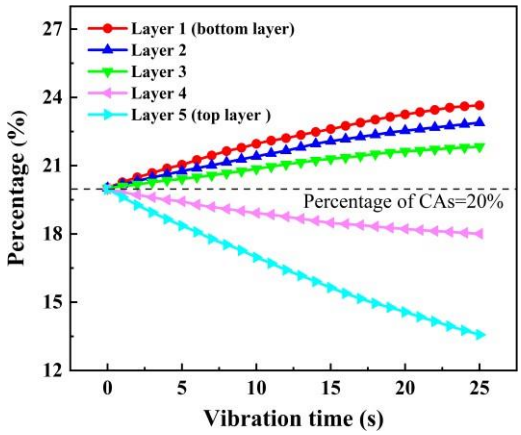

Figure 5. The CA volume percentages of these five layers.

4.2. Effect of CA settlement on chloride transport

Considering that a long-term and long-path transport process is conducive to a more comprehensive investigation on the effect of vibration-induced CA settlement on the transportation of chloride ions, the testing age is set as 10 years and the chloride profile distribution in the section from the middle of concrete specimen and perpendicular to the ionic transport direction is selected for discussion in this study. At the chloride penetration depth of 75 mm, the effect of vibration time on the distribution of chloride concentration along the height direction of concrete specimen is shown in Figure 6.

It could be clearly seen from Figure 6 that with the increase of vibration time, the CA content in the bottom part of concrete specimen increased gradually, leading to a downward trend of chloride concentration in this area after concrete hardening. This was because the tortuous effect and dilution effect reduced the diffusion and transport performance of chloride ions in the bottom part of concrete due to the deposition of more CAs in this area (Liu et al., 2018). Furthermore, the CA content decreased with the increase of the height of concrete specimen, resulting in a significant increase in the chloride concentration, especially in the area with a height of 50 mm in the top part. This was in accordance with the visual analysis observed in Figure 4. When the vibration time was 25 s, there were most of mortars and only a few of CAs with small particle sizes in the top part of concrete specimen, which weakened the resistance capability to chloride penetration in this area.

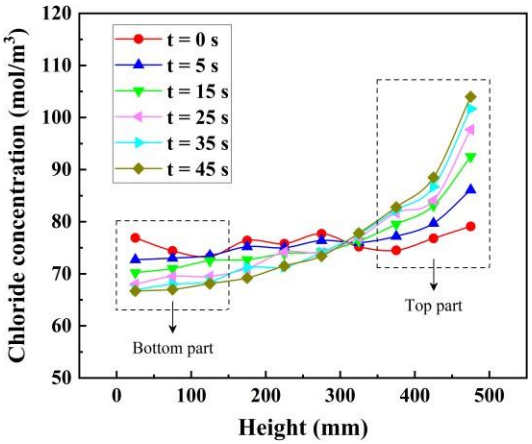

Figure 6. Effect of vibration time on chloride concentration distribution.

In engineering practice, long-time vibration should be avoided, because excessive vibration would aggravate the settlement and segregation of fresh concrete, and the non-uniformity of CA distribution might lead to the earlier deterioration of long-term performance in the top part of hardened concrete due to the chloride contamination with a high concentration in this area. On the contrary, too short vibration time might make it difficult for each component in mixtures to combine closely and entrapped air voids could not be completely removed from the surface of specimen, which also might affect the quality of hardened concrete. Therefore, when casting fresh concrete, the vibration time should be strictly controlled.

4.3. Prediction of time for reinforcement corrosion initiation

Chloride-induced corrosion of steel bars is the primary factor affecting the durability of reinforced concrete structures. In the marine environment or as a consequence of using de-icing salt, chloride ions penetrate into the surface of embedded steel bars through the concrete cover. Once the chloride content around the steel bars reaches a threshold level, reinforcement corrosion begins to occur through a depassivation process, leading to serious damage to the reinforced concrete (Angst et al., 2009; Liu et al., 2021; Zhang et al., 2022). Hence, it is possible to use the proposed numerical model to predict the long-term chloride transport and its effect on the corrosion initiation of steel bars in concrete. The reinforced concrete specimen was simulated to be immersed in 5 wt% sodium chloride solution, and three steel bars were cast horizontally in the top, middle and bottom heights (450 mm, 250 mm and 50 mm), respectively. Here, only one side was treated

as the exposed surface, and the steel bars were arranged in the middle of specimen and perpendicular to the direction of chloride transportation. It meant the chloride concentration at the penetration depth of 75 mm could be approximately regarded as the chloride content near the surface of steel bars.

The development of chloride concentration at the surface of steel bars with immersion time is presented in Figure 7. Note that since the vibration time in practical applications is usually 15–35 s, Figure 7 only shows the prediction results of vibrating durations of 15 s, 25 s and 35 s. As observed, the chloride concentration of the top steel bar was always higher than that of the middle and bottom steel bars at the same testing age. From the result, it could be considered that the reinforcing steel arranged in the top part of specimen tended to corrode earlier.

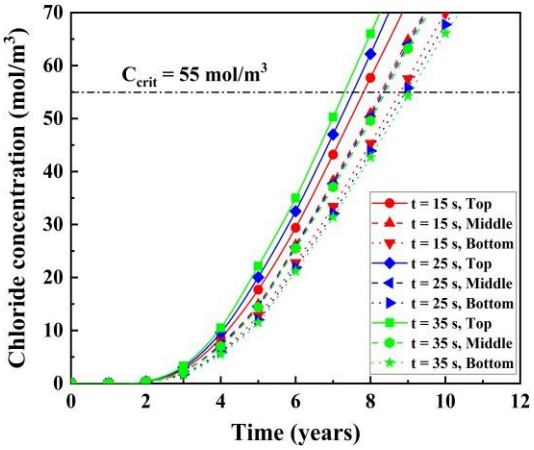

Figure 7. Long-term development of chloride concentration at the surface of steel bars.

In order to quantitatively describe the effect of CA settlement on the corrosion initiation time of steel bars, the critical chloride level of reinforcement corrosion was assumed to be 55 mol/m³. The prediction results for the corrosion initiation time of steel bars in concrete is summarized in Table 2. The model prediction results indicated that the corrosion of the top steel bar initiated 1.03–1.80 years earlier than that of the bottom steel bar under different vibration time. This was because chloride ions penetrated into concrete faster at a higher position due to CA settlement, which was one of the important reasons for the earlier corrosion initiation of reinforcement. Nowadays, much attention has been paid on the mix proportion, binder composition and some special admixtures to improve the durability of reinforced concrete. But in addition to that, more attention should also be paid on the stability of fresh concrete and compacting procedure on site to avoid obvious CA settlement induced by vibration.

Table 2. Prediction of initiation time of reinforcement corrosion in concrete.

Group	Vibration time	Reinforcing steel position	Corrosion initiation time
1	15 s	Top	7.79 years
2	15 s	Middle	8.30 years
3	15 s	Bottom	8.82 years
4	25 s	Top	7.50 years
5	25 s	Middle	8.36 years
6	25 s	Bottom	8.96 years
7	35 s	Top	7.27 years
8	35 s	Middle	8.41 years
9	35 s	Bottom	9.07 years

5. CONCLUSIONS

In this study, a 3-D concrete model is developed to numerically study the vibration-induced CA settlement and its effect on long-term chloride transport in concrete. The results indicate that with the increase of vibration time, a decrease of chloride concentration appears in the bottom part of concrete specimen and a significant increase in the top part, because more CAs deposit to the bottom layer. Due to the sedimentation, a more obvious fluctuation of chloride concentration along the height direction of concrete specimen can be observed with the increase of vibration time. The model prediction results of reinforcement corrosion initiation demonstrate that the corrosion of the top steel bar initiates 1.03–1.80 years earlier than that of the bottom steel bar under different vibration time. In practical engineering, special attention should be paid on the stability of fresh concrete and compacting procedure to avoid the obvious CA settlement during the vibration.

ACKNOWLEDGMENTS

This work was financially supported by the Natural Science Foundation of China (51978396), Natural Science Foundation of Shanghai Municipality, China (22ZR1431400), Natural Science Foundation of Chongqing Municipality, China (No. cstc2021jcyj- msxmX1103), and Oceanic Interdisciplinary Program of Shanghai Jiao Tong University (SL2021MS016).

REFERENCES

1. Angst U., Elsener B., Larsen C.K., Vennesland Ø., 2009. Critical chloride content in reinforced concrete - A review. Cement and Concrete Research, 39(12):1122–1138.
2. Ashraf, M., Iqbal, M.F., Rauf, M., Ashraf, M.U., Ulhaq, A., Liu, Q.F., 2022. Developing a sustainable concrete incorporating bentonite clay and silica fume: Mechanical

and durability performance. Journal of Cleaner Production, 337, 130315.
3. Banfill P.F.G., Xu Y., Domone P.L.J., 1999. Relationship between the rheology of unvibrated fresh concrete and its flow under vibration in a vertical pipe apparatus. Magazine of Concrete Research, 51(3):181–190.
4. Benaicha M., Jalbaud O., Roguiez X., Alaoui A.H., Burtschell Y., 2015. Prediction of Self-Compacting Concrete homogeneity by ultrasonic velocity. Alexandria Engineering Journal, 54(4):1181–1191.
5. Cai Y., Liu Q.F., Yu L., Meng Z., Hu Z., Yuan Q., Savija B., 2021. An experimental and numerical investigation of coarse aggregate settlement in fresh concrete under vibration. Cement and Concrete Composites, 122:104153.
6. Cai Y., Zhang W., Yu L., Chen M., Yang C., François R., Yang K., 2020. Characteristics of the steel-concrete interface and their effect on the corrosion of steel bars in concrete. Construction and Building Materials, 253:119162.
7. Chen W.K., Liu Q.F., 2021. Moisture and multi-ions transport in concrete under drying-wetting cycles: a numerical study. Journal of Hydraulic Engineering, 52(5):622–632.
8. Du X., Jin L., Zhang R., 2015. Chloride diffusivity in saturated cement paste subjected to external mechanicalloadings. Ocean Engineering, 95: 1–10.
9. Gao X., Zhang J., Su Y., 2019. Influence of vibration- induced segregation on mechanical property and chloride ion permeability of concrete with variable rheological performance. Construction and Building Materials, 194:32–41.
10. Gokce H.S., Ozturk B.C., Çam N.F., Andiç-Çakir O., 2018. Gamma-ray attenuation coefficients and transmission thickness of high consistency heavyweight concrete containing mineral admixture. Cement and Concrete Composites, 92:56–69.
11. Hu Z., Liu Q.F., 2023. Numerical study of multi-species transport in cracked concrete under external load. Materials Reports, 37(9):21120077.
12. Khayat K.H., Pavate T.V., Assaad J., Jolicoeur C., 2003. Analysis of variations in electrical conductivity to assess stability of cement-based materials. ACI Materials Journal, 100(4):302–310.
13. Li L.J., Liu Q.F., Tang L., Hu Z., Wen Y., Zhang P., 2021.
Chloride penetration in freeze-thaw induced cracking concrete: A numerical study. Construction and Building Materials, 302:124291.
14. Li L.J., Liu Q.F., 2022. Freezing Rate and Chloride Transport in Concrete Subjected to Freeze-Thaw Cycles: A Numerical Study. Journal of the Chinese Ceramic Society, 50 (8), 10.14062/j.issn.0454-5648.20211102.
15. Liu Q.F., Easterbrook D., Yang J., Li L.Y., 2015. A three- phase, multi-component ionic transport model for simulation of chloride penetration in concrete. Engineering Structures, 86:122–133.
16. Liu Q.F., Feng G.L., Xia J., Yang J., Li L.Y., 2018. Ionic transport features in concrete composites containing
various shaped aggregates: a numerical study. Composite Structures, 183:371–380.
17. Liu Q.F., Hu Z., Wang X.E., Zhao H., Qian K., Li L.J., Meng Z., 2022. Numerical study on cracking and its effect on chloride transport in concrete subjected to external load. Construction and Building Materials, 325:126797.
18. Liu Q.F., Iqbal M.F., Yang J., Lu X.Y., Zhang P., Rauf M., 2021. Prediction of chloride diffusivity in concrete using artificial neural network: Modelling and performance evaluation. Construction and Building Materials, 268:121082.
19. Meng Z., Liu Q.F., She W., Cai Y., Yang J., Iqbal M.F., 2021. Electrochemical deposition method for load-induced crack repair of reinforced concrete structures: A numerical study. Engineering Structures, 246:112903.
20. Meng, Z., Liu, Q.F., Xia, J., Cai, Y., Zhu, X., Zhou, Yu, Pel, L., 2022. Mechanical–transport–chemical modeling of electrochemical repair methods for corrosion-induced cracking in marine concrete. Computer-Aided Civil and Infrastructure Engineering, doi:10.1111/mice.12827.
21. Navarrete I., Lopez M., 2017. Understanding the relationship between the segregation of concrete and coarse aggregate density and size. Construction and Building Materials, 149:741–748.
22. Panesar D.K., Shindman B., 2012. The effect of segregation on transport and durability properties of self consolidating concrete. Cement and Concrete Research,42:252–264.
23. Petrou M.F., Harries K.A., Gadala-Maria F., Kolli V.G., 2000. A unique experimental method for monitoring aggregate settlement in concrete. Cement and Concrete Research, 30(5):809–816.
24. Roussel N., 2006. A theoretical frame to study stability of fresh concrete. Materials and Structures, 39(1):81–91.
25. Sergi G., Yu S.W., Page C.L., 1992. Diffusion of chloride and hydroxyl ions in cementitious materials exposed to a saline environment. Magazine of Concrete Research, 44(158):63–69.
26. Yu Y., Gao W., Feng Y., Castel A., Chen X., Liu A., 2021. On the competitive antagonism effect in combined chloride-sulfate attack: A numerical exploration. Cement and Concrete Research, 144:106406.
27. Zhang C.L., Liu Q.F., 2022. Coupling erosion of chlorides and sulfates in reinforced concrete: a review. Materials Reports, 36(1):20100075.
28. Zheng J., Zhou X., 2008. Analytical solution for the chloride diffusivity of hardened cement paste. Journal of Materials in Civil Engineering, 20(5):384–391.